ACS OMEGA

http://pubs.acs.org/journal/acsodf

Article

First-Principles Study of Three-Dimensional Electrides Containing One-Dimensional $[Ba_3N]^{3+}$ Chains

Xiangyu Zhang, Yunlei Chen, Yongfang Sun, Tian-Nan Ye,* and Xiao-Dong Wen*

Cite This: *ACS Omega* 2022, 7, 13290−13298

Read Online

ACCESS | Metrics & More | Article Recommendations | Supporting Information

ABSTRACT: Electrides, a unique type of compound where electrons act as anions, have a high electron mobility and a low work function, which makes them promising for applications in electronic devices and high-performance catalysts. The discovery of novel electrides and the expansion of the electride family have great significance for their promising applications. Herein, we reported four three-dimensional (3D) electrides by coupling crystal structure database searches and first-principles electronic structure analysis. Subnitrides (Ba_3N, $LiBa_3N$, $NaBa_3N$, and Na_5Ba_3N) containing one-dimensional (1D) $[Ba_3N]^{3+}$ chains are identified as 3D electrides for the first time. The anionic electrons are confined in the 3D interstitial space of Ba_3N, $LiBa_3N$, $NaBa_3N$, and Na_5Ba_3N. Interestingly, with the increase of Na content, the excess electrons of Na_5Ba_3N play two roles of metallic bonding and anionic electrons. Therefore, the subnitrides containing 1D $[Ba_3N]^{3+}$ chains can be regarded as a new family of 3D electrides, where anionic electrons reside in the 3D interstitial spaces and provide a conduction path. These materials not only are experimentally synthesizable 3D electrides but also are promising to be exfoliated into advanced 1D nanowire materials. Furthermore, our work suggests a discovery strategy of novel electrides based on one parent framework like $[Ba_3N]^{3+}$ chains, which would accelerate the mining of electrides from the crystal structure database.

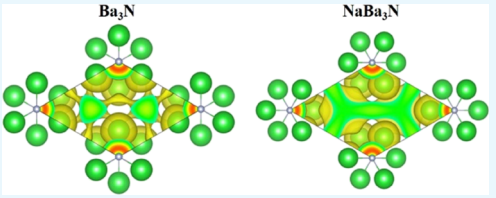

1. INTRODUCTION

Electrides are a unique type of compound in which electrons occupy interstitial space and serve as anions.[1,2] Therefore, electrides exhibit a variety of unique properties, such as high electron mobility and low work function, which makes them promising for applications in electronic devices and high-performance catalysts.[3] According to the dimensions of anionic electrons, electrides can be classified into zero-dimensional (0D), one-dimensional (1D), two-dimensional (2D), and three-dimensional (3D) electrides.[4] Until now, 167 materials from the Inorganic Crystal Structure Database (ICSD) have been identified as electrides by automated screening, including 77 0D, 52 1D, and 38 2D electrides.[5] However, 3D electrides from the ICSD have not been reported. In this work, we look for 3D electrides in the subnitride system from the ICSD.

The alkali-earth metal subnitrides have gained a lot of curiosity recently because of their special electronic structure.[6,7] Unlike common inorganic compounds, the standard rules of valency are invalid for subnitrides since the number of electrons is more than the expected based on well-established electron counting rules.[8] One typical example of subnitrides is Ca_2N, which was determined as a layered structure of the anti-$CdCl_2$ type using single-crystal X-ray diffraction in 1968.[9] Sr_2N is isostructural with Ca_2N and was identified by Gaudé et al. in 1972.[10] Although both of the subnitrides were reported early but their electronic properties had not been revealed until recent years. In 2000, Gregory et al. confirmed that Ca_2N is metallic and paramagnetic at room temperature.[11] In 2013, Lee et al. demonstrated that Ca_2N is a 2D electride in which conduction electrons are confined between $[Ca_2N]^+$ layers with a concentration in good agreement with the chemical formula $[Ca_2N]^+ \cdot e^-$.[6] The 2D nature of its electronic structure was confirmed by both transport measurements and a band calculation. Ca_2N can be exfoliated into 2D nanosheets using liquid exfoliation.[12] Moreover, Ca_2N has a very small work function, making it attractive for use as an electron donor.[13−16] Shortly afterward, Walsh and Scanlon calculated the electronic structures of Sr_2N and Ba_2N and showed that they are also 2D electrides similar to Ca_2N.[8]

Another typical example of subnitrides is Ba_3N, which was synthesized under harsh reaction conditions by Steinbrenner and Simon in 1998.[17] Ba_3N crystallizes in the anti-TiI_3 structure type, and represents a hexagonal close packing of $^1_\infty[NBa_{6/2}]$ chains. Actually, the first subnitride of Ba and Na, $NaBa_3N$, was reported by Rauch and Simon as early as 1992.[18] The thermal decomposition of $NaBa_3N$ under high vacuum could form Ba_3N.[17] In the hexagonal structure of $NaBa_3N$, the Ba and N atoms form $^1_\infty[NBa_{6/2}]$ chains, while single Na atoms are arranged between these chains. In 1995, Snyder and Simon reported another subnitride of Ba and Na, Na_5Ba_3N.[19] Its

Received: February 16, 2022
Accepted: March 23, 2022
Published: April 6, 2022

https://doi.org/10.1021/acsomega.2c00956
ACS Omega 2022, 7, 13290−13298

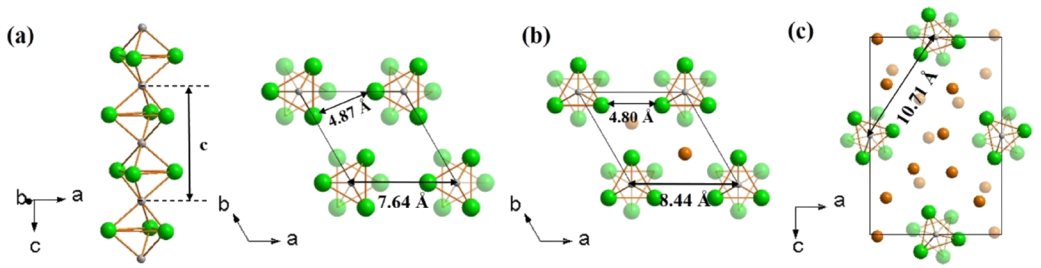

Figure 1. Structure of Ba_3N (a) and $NaBa_3N$ (b) as viewed along the *c*-axis and Na_5Ba_3N (c) as viewed along the *b*-axis. A side view of an isolated $^1_\infty[NBa_{6/2}]$ chain is also shown in (a). The green, gray, and orange spheres, respectively, denote Ba, N, and Na atoms.

structure contains $^1_\infty[NBa_{6/2}]$ chains nearly identical with those found in $NaBa_3N$. In 2007, Smetana et al. reported two subnitrides of Ba and Li, $LiBa_2N$ and $LiBa_3N$. $LiBa_2N$ has a tetragonal structure (space group, $P4_2/nmc$), and its structure contains infinite mutually perpendicular rows of edge-sharing NBa_5Li octahedra, and $LiBa_3N$ is isostructural with $NaBa_3N$.[20] The subnitrides of alkaline earth metals and alkali metals are still being excavated these years,[21−26] although all subnitrides are both air- and water-sensitive.

There is continuing interest in the electronic properties of the subnitrides.[27−29] Recently, Park et al. reported that Ba_3N is identified as a new electride via first-principles calculation and claimed that anionic electrons are aligned in a 1D manner along an interstitial channel.[30] Zhou et al. carried out a first-principles calculation of $LiBa_2N$, identifying it as a new electride, wherein both of Ba and Li provide anionic electrons in different distributions, yielding $LiBa_2N$ a unique electride with a coexistence of 1D and 0D anionic electrons.[31] The objective of the present work is to demonstrate that the Ba_3N, $LiBa_3N$, $NaBa_3N$, and Na_5Ba_3N subnitrides containing $^1_\infty[NBa_{6/2}]$ chains are identified as 3D electrides through detailed electronic structure analysis including the electron localization function (ELF), band structure, density of states (DOS), partial charge density, and work function. Furthermore, our work suggests a discovery strategy of novel electrides based on one parent framework like $[Ba_3N]^{3+}$ chains, which may accelerate the discovery of more novel electride family.

2. CALCULATION METHODS

Density functional theory (DFT) calculations were implemented using the generalized gradient approximation (GGA) Perdew−Burke−Ernzerhof (PBE) functional,[32] and the projected augmented plane-wave (PAW) method[33] was implemented using the Vienna Ab-initio Simulation Package (VASP) code. We also employed a van der Waals (vdW) scheme corrected on top of the PBE functional (PBE-D2,[34] PBE-D3,[35] and PBE-dDsC[36]). The plane-wave basis-set cutoff was set to 500 eV. Self-consistent solutions of the Kohn−Sham equations were obtained by employing 2 × 2 × 2 Monkhorst-Pack grids of k-points to perform integration over the Brillouin zone.[37] Relaxed atomic positions were obtained by using the total energy and force minimization methods. The convergence criterion of energy and force is 2×10^{-5} eV and 0.02 eV/Å. The full electronic DOS was also calculated with a high k-point sampling of 4 × 4 × 4. The ELF[38] was calculated to determine whether the electrons were confined in the interstitial space.

3. RESULTS AND DISCUSSION

3.1. Structures. Ba_3N crystallizes in the hexagonal space group $P6_3/mcm$.[17] In the asymmetric unit, there are one unique Ba atom and one unique N atom. Figure 1a shows the crystal structure of Ba_3N along the *c*-axis. The Ba and N atoms form an infinite $^1_\infty[NBa_{6/2}]$ chain along the *c*-axis composed of face-sharing NBa_6 octahedra. The energetic stability of a material against spinodal decomposition in thermodynamics is determined uniquely by convex hull phase diagrams.[39] The formation energies of the Ba−N system are given in Table S1 and Figure S1 in the Supporting Information, all the chemical formulas correspond to experimentally existing stable crystalline materials in the Materials Project database[40] and ICSD. Ba_2N and Ba are the only required reference materials to uniquely determine the thermodynamic stability of Ba_3N. The formation energy of Ba_3N is negative (−7.25 meV/atom) with respect to Ba_2N and Ba, indicating the thermodynamic stability of Ba_3N. Actually, Ba_3N is an experimentally synthesizable material.[17]

$NaBa_3N$[18] and $LiBa_3N$[20] crystallize in the hexagonal space group $P6_3/mmc$. Because $NaBa_3N$ and $LiBa_3N$ are isostructural, only the structure of $NaBa_3N$ will be discussed in detail. In the asymmetric unit of $NaBa_3N$, there are one unique Na atom, one unique Ba atom, and one unique N atom. Figure 1b shows the crystal structure of $NaBa_3N$ along the *c*-axis. The Ba and N atoms form an infinite $^1_\infty[NBa_{6/2}]$ chain along the *c*-axis composed of face-sharing NBa_6 octahedra, with single Na atoms arranged between these parallelly arranged $^1_\infty[NBa_{6/2}]$ chains. The formation energy of $NaBa_3N$ is negative (−17.4 meV/atom) with respect to Ba_3N and Na, indicating the thermodynamic stability of $NaBa_3N$. In fact, $NaBa_3N$ has been synthesized experimentally.[18] Note that there is a $\pi/6$ rotation of the $^1_\infty[NBa_{6/2}]$ chain of $NaBa_3N$ with respect to those of Ba_3N. The distance between chains of $NaBa_3N$ (8.44 Å) is significantly larger than that of Ba_3N (7.64 Å), while the smallest chain-chain bond length of $NaBa_3N$ (4.80 Å) is close to that of Ba_3N (4.87 Å). However, in the ionic compound Ba_3NBi,[41] which is isostructural with $NaBa_3N$, the distance between chains (7.61 Å) is almost the same as that of Ba_3N (7.64 Å), while the smallest chain-chain bond length (3.95 Å) is significantly smaller than that of Ba_3N (4.87 Å). These results indicate that $NaBa_3N$ is not a common ionic compound.

Na_5Ba_3N crystallizes in the orthorhombic space group *Pnma*.[19] In the asymmetric structure, there are four unique Na atoms, three unique Ba atoms, and one unique N atom. The crystal structure of Na_5Ba_3N, projected along the *b*-axis is shown in Figure 1c. The infinite $^1_\infty[NBa_{6/2}]$ chains along the *b*-axis are very similar to those in $NaBa_3N$, but slightly distorted. The difference is the presence of more Na atoms in the areas

https://doi.org/10.1021/acsomega.2c00956
ACS Omega 2022, 7, 13290−13298

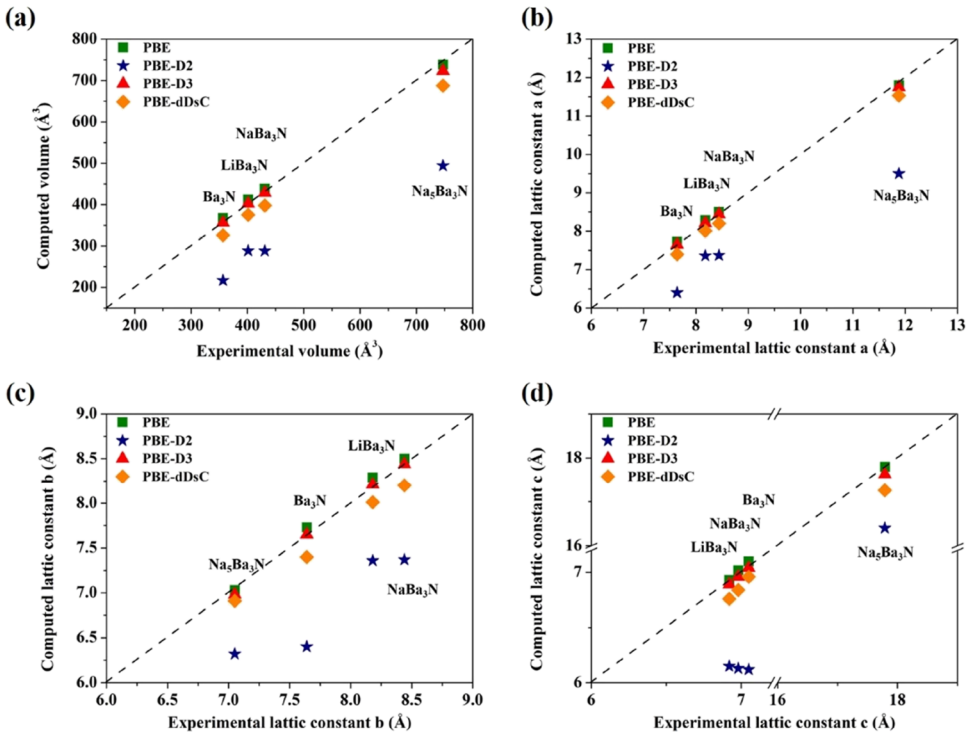

Figure 2. Computed lattice constants (PBE, PBE-D2, PBE-D3, and PBE-dDsC) versus experimental lattice constants including volume (a), lattice constant a (b), lattice constant b (c), and lattice constant c (d) of Ba_3N,[17] $LiBa_3N$,[20] $NaBa_3N$,[18] and Na_5Ba_3N.[19]

between the $^1_\infty[NBa_{6/2}]$ chains in Na_5Ba_3N, as compared to $NaBa_3N$, which leads to the distance between chains of Na_5Ba_3N (10.71 Å) to be much larger than $NaBa_3N$ (8.44 Å). The formation energy of Na_5Ba_3N is negative (−9.11 meV/atom) with respect to Ba_3N and Na, indicating the thermodynamic stability of Na_5Ba_3N. Actually, Snyder and Simon have synthesized Na_5Ba_3N experimentally.[19]

The nearest Ba−Ba interatomic distance (4.87 Å) between the $^1_\infty[NBa_{6/2}]$ chains in Ba_3N is 0.53 Å greater than that in the elemental metal Ba (4.34 Å), which excludes the possibility of direct Ba−Ba bonding. The bond length is another indication supporting ionic bonding characteristic.[6,39] Within the $^1_\infty[NBa_{6/2}]$ chain of Ba_3N, the bond lengths of Ba−N are extremely close to the sum of the respective ionic radii. The Ba−N bond length is 2.726 Å, which is in close proximity to the sum of the ionic radii of Ba^{2+} (1.35 Å) and N^{3-} (1.46 Å). The $^1_\infty[NBa_{6/2}]$ chain of Ba_3N can be regarded as a positively charged ionic chain, $[(Ba^{2+})_3N^{3-}]^{3+}$. To compensate for the positive charge of the $[Ba_3N]^{3+}$ chains, the interstitial space of Ba_3N should work as a confinement space for the anionic electrons, resulting in a $[Ba_3N]^{3+}\cdot 3e^-$ configuration. Within the $^1_\infty[NBa_{6/2}]$ chain of $LiBa_3N$, $NaBa_3N$, and Na_5Ba_3N, the bond lengths of Ba−N are also close to the sum of the respective ionic radii. The Ba−N bond lengths of $LiBa_3N$, $NaBa_3N$, and Na_5Ba_3N are, respectively, 2.722, 2.734, and 2.729−2.746 Å. The $^1_\infty[NBa_{6/2}]$ chain of $LiBa_3N$, $NaBa_3N$, and Na_5Ba_3N also can be regarded as a positively charged ionic chain, $[Ba_3N]^{3+}$. In addition, the insertion of alkali metals leads to a larger distance between chains. Therefore, it is natural to speculate that $LiBa_3N$, $NaBa_3N$, and $NaBa_3N$ formed by intercalating alkali metals (Li or Na) into Ba_3N may be also generate electrides.

Because the interaction between $[Ba_3N]^{3+}$ chains of Ba_3N, $LiBa_3N$, $NaBa_3N$, and Na_5Ba_3N involves both electron interaction and vdW interaction, we employed three vdW correction methods (PBE-D2, PBE-D3, and PBE-dDsC) corrected on top of the PBE functional to elucidate the role of vdW interactions in stabilizing structures and to confirm the accuracy of PBE structure optimization. The results are listed in Table S2 in the Supporting Information. Figure 2 shows the plotted linear correlations between the computed lattice constants and corresponding experimental values.[17−20] For Ba_3N, $LiBa_3N$, and $NaBa_3N$, the lattice constants computed by using the PBE-D3-corrected PBE functional are closest to the experimental values, and for Na_5Ba_3N, the lattice constants computed by using the PBE functional are closest to the experimental values. The absence of imaginary frequency in the phonon dispersion diagrams for Ba_3N, $NaBa_3N$, and Na_5Ba_3N confirm the dynamic stability of structures closest to the experimental value as shown in Figure S2 in the Supporting Information. The structure model closest to the experimental value is used for subsequent electronic property calculation.

3.2. Electronic Structures. Ba_3N has been identified as an electride, whereas a detailed analysis of the electronic properties of Ba_3N is still scarce.[30] Therefore, we calculated its ELF, band structure, DOS, and partial charge density. The ELF isosurface and map of Ba_3N in Figure 3 indicates a pronounced electron localization distributed in the 3D interstitial space between $[Ba_3N]^{3+}$ chains. No electrons are observed between the electron localization space and the $[Ba_3N]^{3+}$ chains, substantiating the ionic bonding nature between the anionic state and the $[Ba_3N]^{3+}$ chains, which is similar to the Ca_2N[6] cases. The difference is that in Ba_3N, the anionic electrons are distributed in the 3D space between $[Ba_3N]^{3+}$ chains, while in Ca_2N, they are distributed in the 2D space between $[Ca_2N]^+$ layers. To further confirm the electride nature of Ba_3N, we artificially constructed three structures (Ba_3N-e^-, Ba_3N-$2e^-$, and Ba_3N-$3e^-$) by removing three

https://doi.org/10.1021/acsomega.2c00956
ACS Omega 2022, 7, 13290−13298

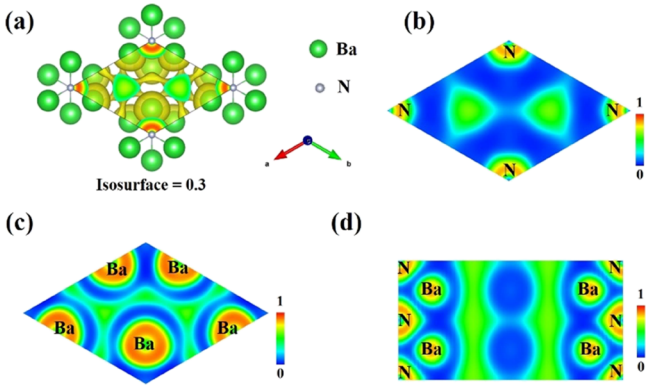

Figure 3. ELF for Ba_3N. The isosurface plot (a) and the corresponding map of the (0001) plane at c = 1 (b), the (0001) plane at c = 3/4 (c), and the $(11\bar{2}0)$ plane (d).

electrons from the primitive cell of Ba_3N one by one and calculated their ELF (Figure S3 in the Supporting Information).[42,43] It shows that with the removal of electrons, the confined electrons gradually decrease until all disappear.

The calculated electronic band structures and projected densities of states (PDOSs) of Ba_3N are plotted in Figure 4a,b. The existence of bands crossing the Fermi level in Figure 4a suggests its metallic characteristics. Figure 4b shows that the bands between −2.6 and −1.5 eV below the Fermi level are predominantly formed by the N 2p orbitals with the Ba 5p

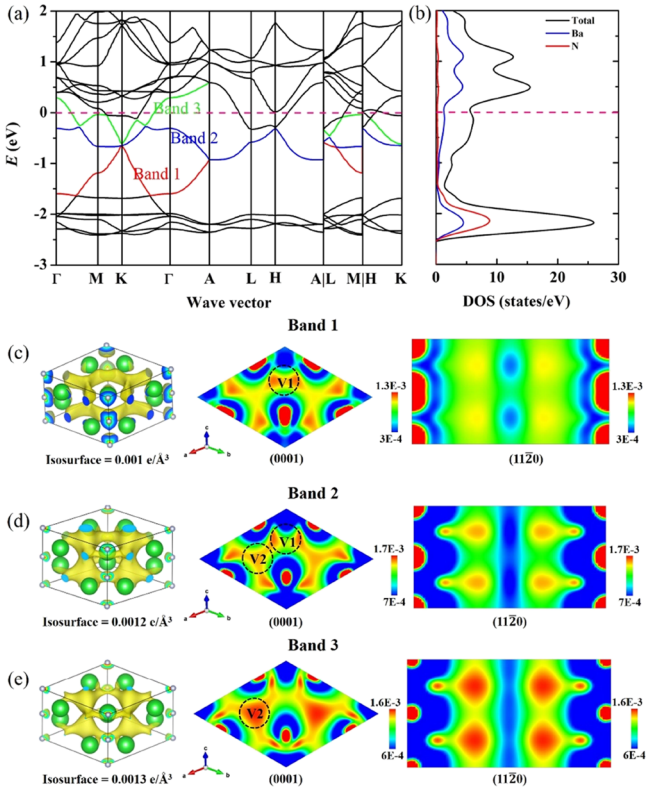

Figure 4. Calculated band structure (a), PDOS (b), the isosurface and the map of partial charge density of interstitial band 1 (c), band 2 (d), and band 3 (e) of Ba_3N. The bands around the Fermi level, mainly contributed by the interstitial electrons, are highlighted in red, blue, and green lines. In (c−e), the green and gray spheres, respectively, denote Ba and N atoms.

orbitals, and bands above the Fermi level are determined the unoccupied Ba 6s orbitals, while the contributions from the atomic orbitals of Ba and N near the Fermi level (between −1.5 and 0 eV) are smaller.

The contributions from the interstitial sites are dominant around the Fermi level, which is a typical character of electrides.[44] However, due to the connection with neighboring bands, the band structure around the Fermi level of Ba_3N is more complicated than other known electrides. In Ca_2N,[6] for example, there is only one band near the Fermi level. Therefore, the existence of the interstitial electrons in Ba_3N is confirmed by the decomposed partial charge densities.[45] By plotting the partial charge density of the three bands (Figure 4c−e) around the Fermi level, we can clearly find that they correspond to interstitial electrons. The results suggest that the electrons of band 1 mainly accumulate around the V1 site, the electrons of band 2 accumulate around both of the V1 site and the V2 site, and the electrons of band 3 mainly accumulate around the V2 site. Because the anionic electrons in Ba_3N are confined in the 3D interstitial space, Ba_3N can be regarded as a 3D electride according to the classification of inorganic electrides in terms of dimensions of anionic electrons.[4] Ca_2N can be exfoliated into 2D nanosheets because layers of atoms are separated by layers of a 2D electron gas.[12] Similarly, Ba_3N is promising to be exfoliated into 1D nanowires because chains of atoms are separated by a 3D electron gas.

To further confirm that bands 1, 2, and 3 are contributed by interstitial electrons of Ba_3N, we, respectively, inserted six and four H atoms at the V1 and V2 sites and relaxed. We found that unlike the little lattice changes caused by the insertion of anions in 0D and 1D electrides, large lattice change happened in Ba_3NH_3-V1 and Ba_3NH_2-V2 after relaxation, and the situation is similar to inserting anions into 2D electrides, such as Ca_2N (Table S3 in the Supporting Information). The reason may be that the anionic electrons are confined in the interstitial space formed by the rigid frame in 0D and 1D electrides, only anions matching the interstitial space can be inserted. While 2D and 3D electrides have more flexible frame structures, when anions are inserted, the distance between layers or chains as well as the thickness of layers and the length of chains can be adjusted according to the size of the anion. If the anion is too large or too small, the most stable structure will not retain its original configuration (such as Ca_2NH[46] and Ca_2NF[47]).

The calculated band structure of the artificial Ba_3NH_3-V1 shows that the bands 1, 2, and 3 disappeared after the introduction of H atoms at the V1 sites, and hydrogen-related bands appear at the energy range of around −3.5 to −1.5 eV for H^- (Figure S4a in the Supporting Information). Ba_3NH_3-V1 turned to be a semiconductor with the introduction of H atoms at the V1 sites. The calculated band structure of the artificial Ba_3NH_2-V2 shows that the bands 1−3 disappeared after the introduction of H atoms at the V2 sites, and hydrogen-related bands appear at the energy range of around −4.5 to −2.6 eV for H^-. At the same time, a new band contributed by excess electron appears near the Fermi level (Figure S4b in the Supporting Information). Ba_3NH_2-V2 remains as metal because the excess electrons are still present in Ba_3NH_2-V2. The above results show that bands 1, 2, and 3 of Ba_3N are the contributions of anionic electrons at the V1 and V2 sites.

Because of the interchain electron distribution, Ba_3N is expected to have a low work function. We calculated its work functions on the $(1\bar{1}00)$ plane and the (0001) plane; the

https://doi.org/10.1021/acsomega.2c00956
ACS Omega 2022, 7, 13290−13298

$(1\bar{1}00)$ plane is cleaved parallel to $[Ba_3N]^{3+}$ chains, and the (0001) plane is cleaved perpendicular to $[Ba_3N]^{3+}$ chains. As presented in Figure S5a,b in the Supporting Information, the work functions of Ba_3N exhibit small surface anisotropy with the value 2.45 eV on the $(1\bar{1}00)$ plane and 2.53 eV on the (0001) plane. By contrast, the work function of 2D electrides Ca_2N exhibits large surface anisotropy with the value 3.39 eV on the plane parallel to $[Ca_2N]^+$ layers and 2.35 eV on the plane perpendicular to $[Ca_2N]^+$ layers.[39] The small surface anisotropy of Ba_3N relative to that of Ca_2N further indicates the 3D feature of anionic electrons in Ba_3N. It should be noted that the work function of Ba_3N is smaller than the value of metal Ba (2.7 eV). Such a low work function of Ba_3N makes it promising in applications such as efficient thermionic emitters, low injection-barrier cathodes for organic light-emitting diodes, and high-performance catalysts.

Since there is a $\pi/6$ rotation of $[Ba_3N]^{3+}$ chains of $NaBa_3N$ with respect to those of Ba_3N, we first studied the effect of the rotation of $[Ba_3N]^{3+}$ chains on electron distribution before studying the electronic properties of $NaBa_3N$. We build the rotation structure by removing the Na atom of the $NaBa_3N$ structure and named the rotation structure $NaBa_3N$-Na (Figure S6 in the Supporting Information). The ELF isosurface and map of $NaBa_3N$-Na are shown in Figure 5. The electron

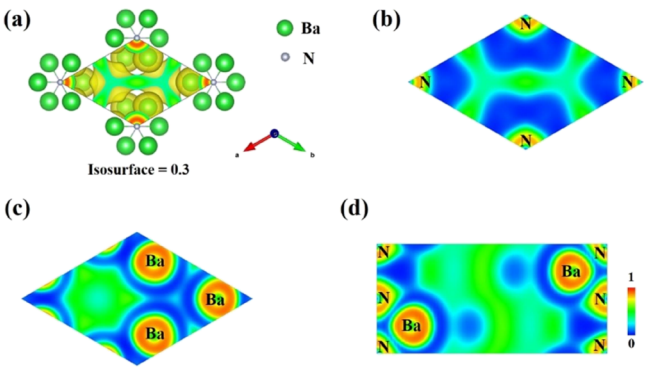

Figure 5. ELF for $NaBa_3N$-Na. The isosurface plot (a) and the corresponding map of the (0001) plane at c = 1 (b), the (0001) plane at c = 3/4 (c), and the $(11\bar{2}0)$ plane (d).

localization of $NaBa_3N$-Na also distributed in the 3D interstitial space between $[Ba_3N]^{3+}$ chains, but the rotation of $[Ba_3N]^{3+}$ chains obviously changes the distribution of localized electrons. Almost no electrons are observed between the electron localization space and the $[Ba_3N]^{3+}$ chains, indicating the ionic bonding nature between the anionic state and the chains, which is the same as the Ba_3N cases. The electron localization also gradually decreases until it disappears as the three excess electrons in the structure of $NaBa_3N$-Na are removed one by one (Figure S7 in the Supporting Information).

The calculated electronic band structures and PDOSs of $NaBa_3N$-Na are plotted in Figure S8a,b in the Supporting Information. Similar to Ba_3N, the bands between −2.8 and −1.5 eV below the Fermi level are predominantly formed by the N 2p orbitals with the Ba 5p orbitals, and bands above the Fermi level are determined the unoccupied Ba 6s orbitals, while the contributions from the atomic orbitals of Ba and N near the Fermi level (between −1.5 and 0 eV) are smaller. The partial charge density of the three bands for $NaBa_3N$-Na around the Fermi level is shown in Figure S8c−e in the Supporting Information, and we can clearly find that they correspond to interstitial electrons. The results suggest that the electrons of band 1 and band 2 mainly accumulate around the V1 site, and the electrons of band 3 mainly accumulate around the V2 site.

When anions (such as Sb^{3-} and Bi^{3-}) are inserted into the rotation structure, Ba_3NX (X = Sb and Bi) is converted into common ionic compounds and becomes a semiconductor.[41] However, if alkali metal atoms (such Li and Na) are inserted into the rotation structure, it may still be an electride. Figure 6

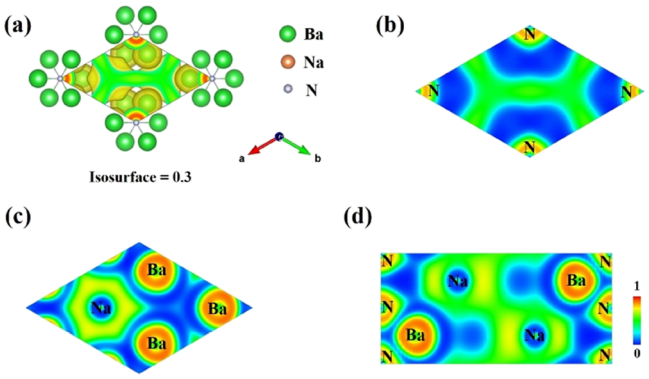

Figure 6. ELF for $NaBa_3N$. The isosurface plot (a) and the corresponding map of the (0001) plane at c = 1 (b), the (0001) plane at c = 3/4 (c), and the $(11\bar{2}0)$ plane (d).

shows the ELF isosurface and map of $NaBa_3N$. The electron localization of $NaBa_3N$ is also distributed in the 3D interstitial space between $[Ba_3N]^{3+}$ chains and the distribution shape of localized electrons is similar to $NaBa_3N$-Na. To further confirm the electride nature of $NaBa_3N$, we artificially constructed four structures ($NaBa_3N$-e^-, $NaBa_3N$-$2e^-$, $NaBa_3N$-$3e^-$, and $NaBa_3N$-$4e^-$) by removing four electrons from the primitive cell of $NaBa_3N$ one by one and calculated their ELF (Figure S9 in Supporting Information). It shows that with the removal of electrons, the confined electrons gradually decrease until they almost disappear.

The calculated electronic band structures and PDOS of $NaBa_3N$ are plotted in Figure 7a,b. The existence of bands crossing the Fermi level in Figure 7a suggests that $NaBa_3N$ is metallic. Compared with $NaBa_3N$-Na, the Fermi level of $NaBa_3N$ moves up. Figure 7b shows that the bands between −1.5 and −2.7 eV below the Fermi level are predominantly formed by the N 2p orbitals with some mixing with the Ba 5p orbitals, and bands between 0.2 and 1 eV above the Fermi level are determined by the unoccupied Ba 6s orbitals, while the contributions from the atomic orbitals of Ba and N near the Fermi level are smaller. By plotting the decomposed partial charge density of the four bands (band 1, 2, 3, and 4) around the Fermi level, we can clearly find that they correspond to interstitial electrons. The results suggest that the electrons of bands 1 and 2 mainly accumulate in the V1 site (between two Ba atoms from the same $[Ba_3N]^{3+}$ chain and one Na), and the electrons of band 3 and 4 mainly accumulate in the V2 site (between two Ba atoms from different $[Ba_3N]^{3+}$ chains and one Na). The results reveal that the anionic electrons in $NaBa_3N$ are confined in the 3D interstitial space. Thus, $NaBa_3N$ also can be regarded as a 3D electride.

To further confirm that bands 1, 2, 3, and 4 are contributed by interstitial electrons of $NaBa_3N$, we, respectively, inserted six H atoms at the V1 and V2 sites and relaxed. As expected,

https://doi.org/10.1021/acsomega.2c00956
ACS Omega 2022, 7, 13290−13298

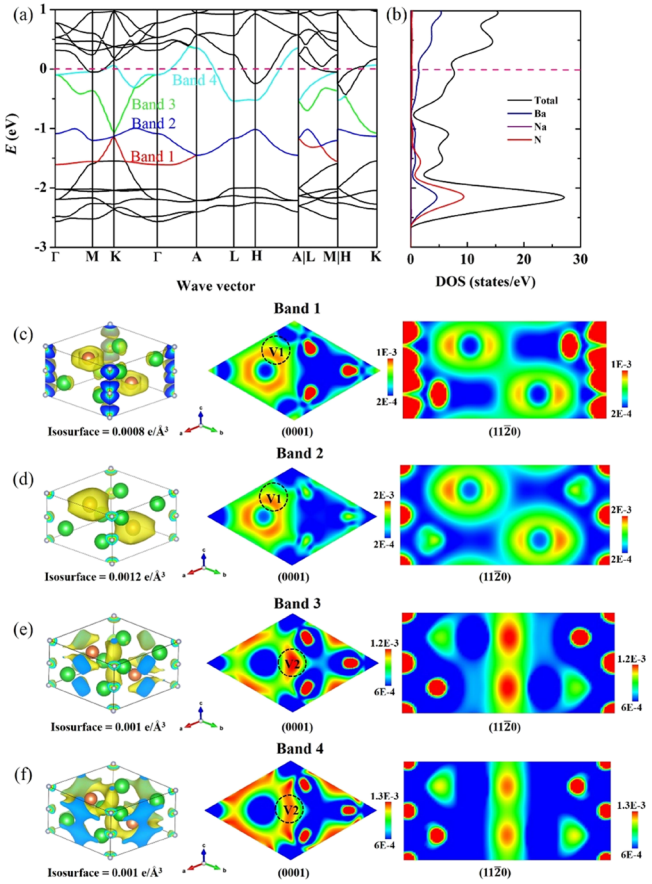

Figure 7. Calculated band structure (a), PDOS (b), the isosurface and the map of partial charge density of interstitial band 1 (c), band 2 (d), band 3 (e), and band 4 (f) of $NaBa_3N$. The interstitial bands, mainly contributed by the interstitial electrons, are highlighted in bold red, blue, green, and cyan lines. In (c–f), the green, gray, and orange spheres, respectively, denote Ba, N, and Na atoms.

large lattice change happened in $NaBa_3NH_3$-V1 and $NaBa_3NH_3$-V2 after relaxation (Table S3 in the Supporting Information). The calculated band structure of the artificial $NaBa_3NH_3$-V1 shows that the bands 1, 2, 3, and 4 disappeared after the introduction of H atoms at the V1 sites, and hydrogen-related bands appear at the energy range of around −3.5 to −1.5 eV for H^-. At the same time, a new band contributed by excess electron appears near the Fermi level (Figure S10a in the Supporting Information). The calculated band structure of the artificial $NaBa_3NH_3$-V2 shows that the band 1, 2, 3, and 4 disappeared after the introduction of H atoms at the V2 sites, and hydrogen-related bands appear at the energy range of around −4.5 to −2.6 eV for H^-. At the same time, a new band contributed by excess electron appears near the Fermi level (Figure S10b in the Supporting Information). The $NaBa_3NH_3$-V1 and $NaBa_3NH_3$-V2 are still metal after the H atoms were introduced at the V1 and V2 sites because the excess electrons are present in $NaBa_3NH_3$-V1 and $NaBa_3NH_3$-V2. The above results show that bands 1, 2, 3, and 4 of $NaBa_3N$ are the contributions of anionic electrons at sites V1 and V2.

We calculated the work functions of $NaBa_3N$ on the (1$\bar{1}$00) plane and the (0001) plane; the (1$\bar{1}$00) plane is cleaved parallel to $[Ba_3N]^{3+}$ chains, and the (0001) plane is cleaved perpendicular to $[Ba_3N]^{3+}$ chains. As presented in Figure S11a,b in the Supporting Information, the work functions of $NaBa_3N$ exhibit small surface anisotropy with the value 2.62 eV on the (1$\bar{1}$00) plane and 2.58 eV on the (0001) plane. The work function of $NaBa_3N$ is smaller than the value of metal Ba (2.7 eV) and Na (2.75 eV). This result further indicates that $NaBa_3N$ is a 3D electride.

Next, we studied the electronic properties of Na_5Ba_3N. The ELF isosurface and map of Na_5Ba_3N with different charge states are plotted in Figure 8. Figure 8e shows that the anionic

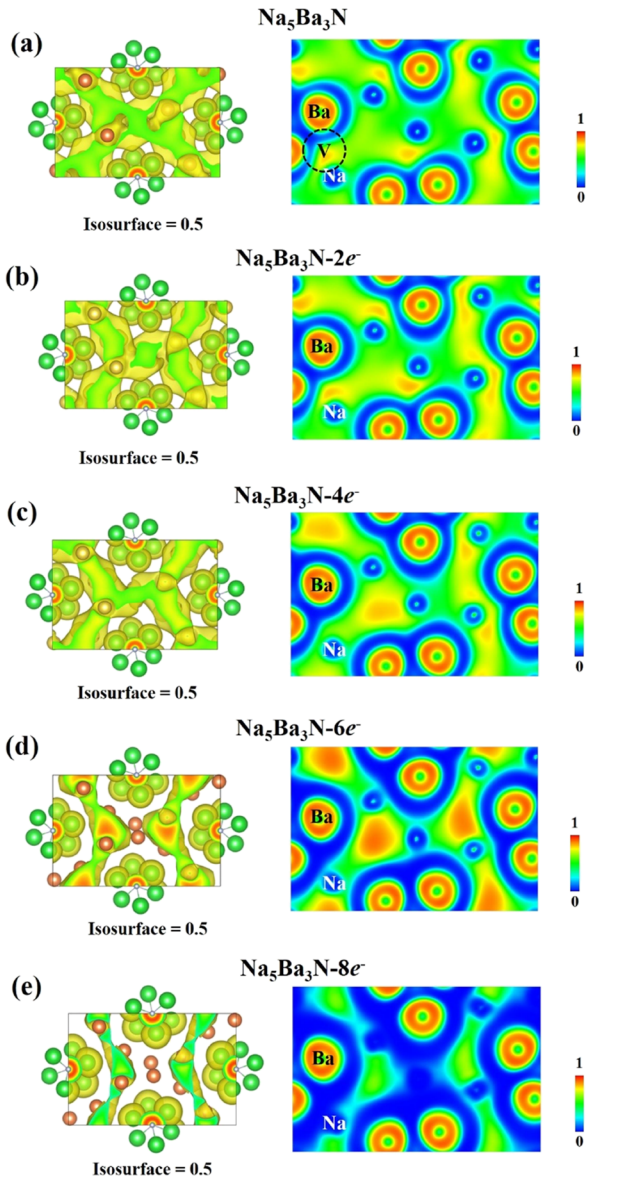

Figure 8. Calculated ELF for Na_5Ba_3N (a), Na_5Ba_3N-2e^- (b), Na_5Ba_3N-4e^- (c), Na_5Ba_3N-6e^- (d), and Na_5Ba_3N-8e^- (e). The isosurface plot (left) and the corresponding map of the (010) plane at c = 3/4 (right). The green, gray, and orange spheres, respectively, denote Ba, N, and Na atoms.

electrons between the Na atom and the $[Ba_3N]^{3+}$ chain (V sites) disappeared after removing eight extra electrons, and the removal of six extra electrons (Figure 8d) shows almost the same ELF distribution except the metallic bonding near Na atoms is enhanced. This reveals that the metallic bonding has stronger ability to attract electrons than V sites. Electron localization appears at V sites with the increase of the number

https://doi.org/10.1021/acsomega.2c00956
ACS Omega 2022, 7, 13290−13298

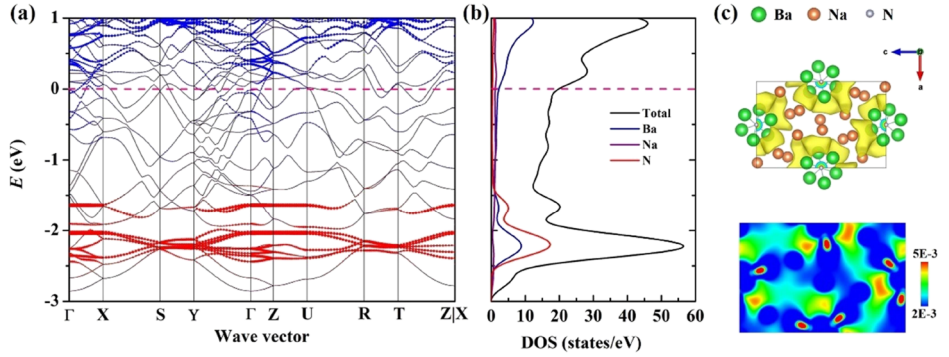

Figure 9. (a) Calculated band structure of Na_5Ba_3N. The Ba-, Na-, and N-related bands are depicted using blue, purple, and red dots. (b) Total and projected DOS of Na_5Ba_3N. (c) Calculated partial charge density for Na_5Ba_3N around the Fermi level (-1.38 eV < $E-E_F$ < 0 eV). The isosurface plot of the partial charge density is set as 0.003 e/Å^3 along the *b*-axis and the corresponding map of the (010) plane at c = 3/4.

of extra electrons (Figure 8a). The result shows that Na_5Ba_3N is different from $NaBa_3N$ and possess mixed ionic and metallic bonding similar to $NaBa_2O$ and $Ca_5Ga_2N_4$.[42]

The calculated electronic band structures and PDOSs of Na_5Ba_3N are plotted in Figure 9a,b. The existence of bands crossing the Fermi level in Figure 9a suggests its metallic characteristics. Figure 9b shows that the bands between -3.0 and -1.4 eV below the Fermi level are predominantly formed by the N 2p orbitals with some mixing with the Ba 5p orbitals, and bands above the Fermi level are determined the unoccupied Ba 6s orbitals, while the contributions from the atomic orbitals of Ba and N near the Fermi level are smaller. The existence of the interstitial electrons in Na_5Ba_3N is further confirmed by the partial charge densities as shown in Figure 9c. Electrons near the Fermi level (-1.38 eV < $E-E_F$ < 0 eV) mainly accumulate between the Na atoms and the $[Ba_3N]^{3+}$ chains.

We calculated the work functions of Na_5Ba_3N on the (001) plane and the (010) plane; the (001) plane is cleaved parallel to $[Ba_3N]^{3+}$ chains, and the (010) plane is cleaved perpendicular to $[Ba_3N]^{3+}$ chains. As presented in Figure S12a,b in the Supporting Information, the work functions of Na_5Ba_3N exhibit small surface anisotropy with the value 2.63 eV on the (010) plane and 2.56 eV on the (001) plane. The work function of Na_5Ba_3N is smaller than the value of metal Ba (2.7 eV) and Na (2.75 eV). This result further indicates that Na_5Ba_3N is a 3D electride.

4. CONCLUSIONS

In summary, we have identified subnitrides (Ba_3N, $LiBa_3N$, $NaBa_3N$, and Na_5Ba_3N) containing 1D $[Ba_3N]^{3+}$ chains as 3D electrides for the first time through ELF, band structure, DOS, partial charge density, and work function calculations. These materials not only are experimentally synthesizable 3D electrides but also are promising to be exfoliated into advanced 1D nanowire materials. Interestingly, $LiBa_3N$, $NaBa_3N$, and Na_5Ba_3N are obtained by inserting alkali metals (Li or Na) into Ba_3N. Therefore, our work also demonstrates that the discovery strategy of novel electrides based on one parent framework like $[Ba_3N]^{3+}$ chains may accelerate the discovery of more novel electrides.

■ ASSOCIATED CONTENT

Supporting Information

The Supporting Information is available free of charge at https://pubs.acs.org/doi/10.1021/acsomega.2c00956.

The formation energies of the Ba−N system, $NaBa_3N$, and Na_5Ba_3N; the convex hulls were reproduced using the DFT calculated energy data for only experimentally already existing compositions for the Ba−N system from the Materials Project database; the lattice constants of Ba_3N, $LiBa_3N$, $NaBa_3N$, and Na_5Ba_3N using different vdW-corrected methods (PBE, PBE-D2, PBE-D3, and PBE-dDsC); phonon dispersion diagrams of Ba_3N, $NaBa_3N$, and Na_5Ba_3N; the ELF for Ba_3N-e^-, Ba_3N-$2e^-$, and Ba_3N-$3e^-$; the lattice constants of electrides before and after the insertion of anions; The calculated band structure, PDOS, and the isosurface of partial charge density for the artificial Ba_3NH_3-V1 and Ba_3NH_2-V2; the Ba_3N work function of the $(1\bar{1}00)$ plane and the (0001) plane together with the corresponding slab models; the construction process of the structure of $NaBa_3N$-Na; the ELF for $NaBa_3N$-Na-e^-, $NaBa_3N$-Na-$2e^-$, and $NaBa_3N$-Na-$3e^-$; The calculated band structure, PDOS, the isosurface, and the map of partial charge density of interstitial band 1, band 2, and band 3 of $NaBa_3N$-Na; the ELF for $NaBa_3N$-e^-, $NaBa_3N$-$2e^-$, $NaBa_3N$-$3e^-$, and $NaBa_3N$-$4e^-$; The calculated band structure, PDOS, and the isosurface of partial charge density for the artificial of $NaBa_3NH_3$-V1 and $NaBa_3NH_3$-V2; the $NaBa_3N$ work function of the $(1\bar{1}00)$ plane and the (0001) plane together with the corresponding slab models; and the Na_5Ba_3N work function of the (001) plane and the (010) plane together with the corresponding slab models (PDF)

■ AUTHOR INFORMATION

Corresponding Authors

Tian-Nan Ye − *Frontiers Science Center for Transformative Molecules, Shanghai Jiao Tong University, Shanghai 200240, China*; Email: ytn2011@sjtu.edu.cn

Xiao-Dong Wen − *State Key Laboratory of Coal Conversion, Institute of Coal Chemistry of CAS, Taiyuan 030001, China; National Energy Center for Coal to Liquids, Synfuels China Co., Ltd, Beijing 101400, China; University of Chinese Academy of Sciences, Beijing 100049, China*; orcid.org/0000-0001-5626-8581; Email: wxd@sxicc.ac.cn

Authors

Xiangyu Zhang − *State Key Laboratory of Coal Conversion, Institute of Coal Chemistry of CAS, Taiyuan 030001, China; National Energy Center for Coal to Liquids, Synfuels China*

https://doi.org/10.1021/acsomega.2c00956
ACS Omega 2022, 7, 13290−13298

Co., Ltd, Beijing 101400, China; University of Chinese Academy of Sciences, Beijing 100049, China

Yunlei Chen − *SINOPEC Shanghai Research Institute of Petrochemical Technology, Shanghai 200120, China*

Yongfang Sun − *State Key Laboratory of Coal Conversion, Institute of Coal Chemistry of CAS, Taiyuan 030001, China; National Energy Center for Coal to Liquids, Synfuels China Co., Ltd, Beijing 101400, China; University of Chinese Academy of Sciences, Beijing 100049, China*

Complete contact information is available at: https://pubs.acs.org/10.1021/acsomega.2c00956

Notes

The authors declare no competing financial interest.

■ ACKNOWLEDGMENTS

The authors are grateful for the financial support from the National Natural Science Foundation of China (Nos. 21972157, 21972160, 21473229, 92045303, 21603252, and 22105122), CAS Project for Young Scientists in Basic Research (YSBR-005), Key R&D plan of Beijing Municipal Science and Technology Commission (Z181100005118014), Key Research Program of Frontier Sciences CAS (ZDBS-LY-7007), Science and Technology Commission of Shanghai Municipality (21PJ1407400), CAS Project for Internet Security and Information Technology (CAS-WX2021SF0110), and funding support from Beijing Advanced Innovation Center for Materials Genome Engineering, Synfuels China, Co. Ltd.

■ REFERENCES

(1) Dye, J. L. Electrides: ionic salts with electrons as the anions. *Science* **1990**, *247*, 663−668.

(2) Liu, C.; Nikolaev, S. A.; Ren, W.; Burton, L. A. Electrides: a review. *J. Mater. Chem. C* **2020**, *8*, 10551−10567.

(3) Hosono, H.; Kitano, M. Advances in materials and applications of inorganic electrides. *Chem. Rev.* **2021**, *121*, 3121−3185.

(4) Tada, T.; Wang, J.; Hosono, H. First principles evolutionary search for new electrides along the dimensionality of anionic electrons. *J. Comput. Chem., Jpn.* **2017**, *16*, 135−138.

(5) Zhu, Q.; Frolov, T.; Choudhary, K. Computational discovery of inorganic electrides from an automated screening. *Matter* **2019**, *1*, 1293−1303.

(6) Lee, K.; Kim, S. W.; Toda, Y.; Matsuishi, S.; Hosono, H. Dicalcium nitride as a two-dimensional electride with an anionic electron layer. *Nature* **2013**, *494*, 336−340.

(7) Oh, J. S.; et al. Evidence for anionic excess electrons in a quasi-two-dimensional Ca_2N electride by angle-resolved photoemission spectroscopy. *J. Am. Chem. Soc.* **2016**, *138*, 2496−2499.

(8) Walsh, A.; Scanlon, D. O. Electron excess in alkaline earth sub-nitrides: 2D electron gas or 3D electride? *J. Mater. Chem. C* **2013**, *1*, 3525−3528.

(9) Keve, E. T.; Skapski, A. C. The crystal structure of dicalcium nitride. *Inorg. Chem.* **1968**, *7*, 1757−1761.

(10) Gaudé, J.; L'Haridon, P.; Laurent, Y.; Lang, J. The system strontium-nitrogen. III. structure study of Sr_2N. *Bull. Soc. fr. Minéral. Cristallogr.* **1972**, *95*, 56−60.

(11) Gregory, D. H.; Bowman, A.; Baker, C. F.; Weston, D. P. Dicalcium nitride, Ca_2N—a 2D ″excess electron″ compound; synthetic routes and crystal chemistry. *J. Mater. Chem.* **2000**, *10*, 1635−1641.

(12) Druffel, D. L.; Kuntz, K. L.; Woomer, A. H.; Alcorn, F. M.; Hu, J.; Donley, C. L.; Warren, S. C. Experimental demonstration of an electride as a 2D material. *J. Am. Chem. Soc.* **2016**, *138*, 16089−16094.

(13) Kim, Y. J.; Kim, S. M.; Cho, E. J.; Hosono, H.; Yang, J. W.; Kim, S. W. Two dimensional inorganic electride-promoted electron transfer efficiency in transfer hydrogenation of alkynes and alkenes. *Chem. Sci.* **2015**, *6*, 3577−3581.

(14) Kitano, M.; Inoue, Y.; Ishikawa, H.; Yamagata, K.; Nakao, T.; Tada, T.; Matsuishi, S.; Yokoyama, T.; Hara, M.; Hosono, H. Essential role of hydride ion in ruthenium-based ammonia synthesis catalysts. *Chem. Sci.* **2016**, *7*, 4036−4043.

(15) Kim, Y. J.; Kim, S. M.; Yu, C.; Yoo, Y.; Cho, E. J.; Yang, J. W.; Kim, S. W. Chemoselective hydrodehalogenation of organic halides utilizing two-dimensional anionic electrons of inorganic electride $[Ca_2N]^+ \cdot e^-$. *Langmuir* **2017**, *33*, 954−958.

(16) Yoo, B. I.; Kim, Y. J.; You, Y.; Yang, J. W.; Kim, S. W. Birch reduction of aromatic compounds by inorganic electride $[Ca_2N]^+ \cdot e^-$ in an alcoholic solvent: an analogue of solvated electrons. *J. Org. Chem.* **2018**, *83*, 13847−13853.

(17) Steinbrenner, U.; Simon, A. Ba_3N - a new binary nitride of an alkaline earth metal. *Z. Anorg. Allg. Chem.* **1998**, *624*, 228−232.

(18) Rauch, P. E.; Simon, A. The new subnitride $NaBa_3N$; an extension of alkali metal suboxide chemistry. *Angew. Chem., Int. Ed.* **1992**, *31*, 1519−1521.

(19) Snyder, G. J.; Simon, A. The infinite chain nitride Na_5Ba_3N. a one-dimensional void metal? *J. Am. Chem. Soc.* **1995**, *117*, 1996−1999.

(20) Smetana, V.; Babizhetskyy, V.; Vajenine, G. V.; Simon, A. Synthesis and crystal structure of $LiBa_2N$ and identification of $LiBa_3N$. *J. Solid State Chem.* **2007**, *180*, 1889−1893.

(21) Snyder, G. J.; Simon, A. Discrete M_6N octahedra in the subnitrides $Na_{16}Ba_6N$ and $Ag_{16}Ca_6N$: a reconsideration of the Ag_8Ca_3 structure type. *Angew. Chem., Int. Ed.* **1994**, *33*, 689−691.

(22) Simon, A.; Steinbrenner, U. Subnitrides with the new cluster $Ba_{14}CaN_6$. *J. Chem. Soc., Faraday Trans.* **1996**, *92*, 2117−2123.

(23) Steinbrenner, U.; Simon, A. $Na_{14}Ba_{14}CaN_6$—a nanodispersion of a salt in a metal. *Angew. Chem., Int. Ed.* **1996**, *35*, 552−554.

(24) Vajenine, G. V.; Steinbrennert, U.; Simon, A. A new subnitride in the series $Na_nBa_{14}CaN_6$ with n = 8. *C. R. Acad. Sci.* **1999**, *2*, 583−589.

(25) Smetana, V.; Babizhetskyy, V.; Vajenine, G. V.; Simon, A. Synthesis and crystal structure of the new quaternary subnitride $Na_{15}Li_8Ba_{12}N_6$. *Z. Anorg. Allg. Chem.* **2007**, *633*, 2296−2299.

(26) Smetana, V.; Babizhetskyy, V.; Simon, A. $Li_xNa_yBa_{14}LiN_6$: new representatives of the subnitride family. *Z. Anorg. Allg. Chem.* **2008**, *634*, 629−632.

(27) Steinbrenner, U.; Adler, P.; Hölle, W.; Simon, A. Electronic structure and chemical bonding in alkaline earth metal subnitrides: photoemission studies and band structure calculations. *J. Phys. Chem. Solids* **1998**, *59*, 1527−1536.

(28) Weiss, H.; Vajenine, G. V.; Steinbrenner, U.; Simon, A.; Balthes, E.; Wyder, P. Fermi surface investigations of the alkaline-earth-metal subnitride $NaBa_3N$ by means of de haas−van alphen oscillations. *Phys. Rev. B* **2001**, *63*, No. 115104.

(29) Oliva, J. M. Subnitride chemistry: a first-principles study of the $NaBa_3N$, Na_5Ba_3N, and $Na_{16}Ba_6N$ phases. *J. Solid State Chem.* **2005**, *178*, 1023−1029.

(30) Park, C.; Kim, S. W.; Yoon, M. First-principles prediction of new electrides with nontrivial band topology based on one-dimensional building blocks. *Phys. Rev. Lett.* **2018**, *120*, No. 026401.

(31) Zhou, J.; Shen, L.; Yang, M.; Cheng, H.; Kong, W.; Feng, Y. P. Discovery of hidden classes of layered electrides by extensive high-throughput material screening. *Chem. Mater.* **2019**, *31*, 1860−1868.

(32) Perdew, J. P.; Burke, K.; Ernzerhof, M. Generalized gradient approximation made simple. *Phys. Rev. Lett.* **1996**, *77*, 3865−3868.

(33) Blochl, P. E. Projector augmented-wave method. *Phys. Rev. B* **1994**, *50*, 17953.

(34) Grimme, S. Semiempirical GGA-type density functional constructed with a long-range dispersion correction. *J. Comput. Chem.* **2006**, *27*, 1787−1799.

(35) Moellmann, J.; Grimme, S. DFT-D3 study of some molecular crystals. *J. Phys. Chem. C* **2014**, *118*, 7615−7621.

(36) Steinmann, S. N.; Corminboeuf, C. Comprehensive benchmarking of a density-dependent dispersion correction. *J. Chem. Theory Comput.* **2011**, *7*, 3567−3577.
(37) Pack, J. D.; Monkhorst, H. J. ″Special points for Brillouin-zone integrations″—a reply. *Phys. Rev. B* **1977**, *16*, 1748.
(38) Savin, A.; Nesper, R.; Wengert, S.; Fässler, T. F. ELF: the electron localization function. *Angew. Chem., Int. Ed.* **1997**, *36*, 1808−1832.
(39) Ming, W.; Yoon, M.; Du, M. H.; Lee, K.; Kim, S. W. First-principles prediction of thermodynamically stable two-dimensional electrides. *J. Am. Chem. Soc.* **2016**, *138*, 15336−15344.
(40) Jain, A.; et al. Commentary: The Materials Project: A materials genome approach to accelerating materials innovation. *APL Mater.* **2013**, *1*, No. 011002.
(41) Gäbler, F.; Kirchner, M.; Schnelle, W.; Schwarz, U.; Schmitt, M.; Rosner, H.; Niewa, R. $(Sr_3N)E$ and $(Ba_3N)E$ (E = Sb, Bi): synthesis, crystal structures, and physical properties. *Z. Anorg. Allg. Chem.* **2004**, *630*, 2292−2298.
(42) Wang, J.; Zhu, Q.; Wang, Z.; Hosono, H. Ternary inorganic electrides with mixed bonding. *Phys. Rev. B* **2019**, *99*, No. 064104.
(43) Sa, B.; Xiong, R.; Wen, C.; Li, Y.-L.; Lin, P.; Lin, Q.; Anpo, M.; Sun, Z. Electronic anisotropy and superconductivity in one-dimensional electride Ca_3Si. *J. Phys. Chem. C* **2020**, *124*, 7683−7690.
(44) Qu, J.; Zhu, S.; Zhang, W.; Zhu, Q. Electrides with dinitrogen ligands. *ACS Appl. Mater. Interfaces* **2019**, *11*, 5256−5263.
(45) Zhu, S.-C.; Wang, L.; Qu, J.-Y.; Wang, J.-J.; Frolov, T.; Chen, X.-Q.; Zhu, Q. Computational design of flexible electrides with nontrivial band topology. *Phys. Rev. Mater.* **2019**, *3*, No. 024205.
(46) Brice, J.-F.; Motte, J.-P.; Courtois, A.; Protas, J.; Aubry, J. Etude structurale de Ca_2NH par diffraction des rayons X, diffraction des neutrons et résonance magnétique nucléaire du proton dans le solide. *J. Solid State Chem.* **1976**, *17*, 135−142.
(47) Jack, D. R.; Zeller, M.; Wagner, T. R. Doubled-cubic Ca_2NF. *Acta Crystallogr. C* **2005**, *C61*, i6−i8.

https://doi.org/10.1021/acsomega.2c00956
ACS Omega 2022, 7, 13290−13298